NEUROSCIENCE

Claustrum mediates bidirectional and reversible control of stress-induced anxiety responses

Misaki Niu[1]†, Atsushi Kasai[1]*†, Masato Tanuma[1], Kaoru Seiriki[1,2], Hisato Igarashi[1], Takahiro Kuwaki[1], Kazuki Nagayasu[1,3], Keita Miyaji[1], Hiroki Ueno[1], Wataru Tanabe[1], Kei Seo[1], Rei Yokoyama[1], Jin Ohkubo[1], Yukio Ago[1,4], Misuzu Hayashida[1], Ken-ichi Inoue[5,6], Masahiko Takada[5], Shun Yamaguchi[7,8], Takanobu Nakazawa[1,9,10], Shuji Kaneko[3], Hiroyuki Okuno[11], Akihiro Yamanaka[12], Hitoshi Hashimoto[1,13,14,15,16]*

The processing of stress responses involves brain-wide communication among cortical and subcortical regions; however, the underlying mechanisms remain elusive. Here, we show that the claustrum (CLA) is crucial for the control of stress-induced anxiety-related behaviors. A combined approach using brain activation mapping and machine learning showed that the CLA activation serves as a reliable marker of exposure to acute stressors. In TRAP2 mice, which allow activity-dependent genetic labeling, chemogenetic activation of the CLA neuronal ensemble tagged by acute social defeat stress (DS) elicited anxiety-related behaviors, whereas silencing of the CLA ensemble attenuated DS-induced anxiety-related behaviors. Moreover, the CLA received strong input from DS-activated basolateral amygdala neurons, and its circuit-selective optogenetic photostimulation temporarily elicited anxiety-related behaviors. Last, silencing of the CLA ensemble during stress exposure increased resistance to chronic DS. The CLA thus bidirectionally controls stress-induced emotional responses, and its inactivation can serve as a preventative strategy to increase stress resilience.

INTRODUCTION

Acute stress leads to a large-scale change in neuronal activity and results in the emergence of negative emotional states, such as anxiety, which promote appropriate behaviors to achieve safety (*1*, *2*); however, excessive and prolonged stress is associated with psychiatric disorders, including anxiety and depression disorders (*3*). The molecular processes underlying stress responses, including spatiotemporal changes of catecholaminergic signals (*1*) and behavioral responses (*2*), require brain-wide communication between the cortical, subcortical, and upper brainstem regions (*4*, *5*). The amygdala, which receives substantial input from sensory domains, can control emotional states and behavioral output (*6*–*8*) and contains neuronal ensembles that can be used to predict changes in brain states, including defensive states (*9*). However, the underlying pathways and mechanisms underpinning stress processing remain to be fully elucidated.

Considerable effort has been devoted to discover brain regions (*5*), circuits (*8*, *10*), and neuronal subsets (*9*, *11*), which are involved in communication among cortical and subcortical regions in stress responses and stress-related disorders, such as depressive disorders. Nevertheless, for example, the downstream pathways of the basolateral amygdala (BLA) (*9*), a critical brain area that regulates emotional behavior, remain elusive. One reason for this may be that, until recently, there have been few unbiased and hypothesis-free approaches for identifying these previously unknown neural elements, particularly due to technical limitations in large-volume imaging, functional genetic labeling, and subsequent group comparisons of normal and disease model brains. Therefore, the identification of such elements remains challenging, especially when the regions are small and consist of only a few cells; nevertheless, such identification will lead to advances in the understanding of stress and its relevant symptoms, as well as effective treatments for these conditions.

Given this background, we have recently developed a whole-brain imaging system named block-face serial microscopy tomography (FAST), which enables unbiased quantitative comparisons of imaging datasets at a subcellular resolution, such as between normal and disease model brains (*12*–*14*). Using FAST, we conducted brain activation mapping in Arc-dVenus mice, in which the expression of dVenus fluorescent protein is driven by the promoter of the immediate early gene *Arc* (*15*), which underwent restraint stress (RS). We observed that the number of activated neurons increased in cerebral cortical areas, the septum, striatum, claustrum (CLA), and amygdaloid nuclei (*12*).

In the present study, we applied brain-wide activation mapping at a single-cell resolution in conjunction with machine learning, activity-dependent genetic labeling, and subsequent manipulation of neuronal functions, so as to investigate the role of activated neurons in the CLA under stress conditions. Intriguingly, we found

[1]Laboratory of Molecular Neuropharmacology, Graduate School of Pharmaceutical Sciences, Osaka University, Osaka, Japan. [2]Institute for Transdisciplinary Graduate Degree Programs, Osaka University, Osaka, Japan. [3]Department of Molecular Pharmacology, Graduate School of Pharmaceutical Sciences, Kyoto University, Kyoto, Japan. [4]Department of Cellular and Molecular Pharmacology, Graduate School of Biomedical and Health Sciences, Hiroshima University, Hiroshima, Japan. [5]Systems Neuroscience Section, Primate Research Institute, Kyoto University, Aichi, Japan. [6]PRESTO, Japan Science and Technology Agency, Saitama, Japan. [7]Department of Morphological Neuroscience, Graduate School of Medicine, Gifu University, Gifu, Japan. [8]Center for Highly Advanced Integration of Nano and Life Sciences, Gifu University, Gifu, Japan. [9]Department of Pharmacology, Graduate School of Dentistry, Osaka University, Osaka, Japan. [10]Department of Bioscience, Tokyo University of Agriculture, Tokyo, Japan. [11]Laboratory of Biochemistry and Molecular Biology, Graduate School of Medical and Dental Sciences, Kagoshima University, Kagoshima, Japan. [12]Department of Neuroscience II, Research Institute of Environmental Medicine, Nagoya University, Nagoya, Japan. [13]Molecular Research Center for Children's Mental Development, United Graduate School of Child Development, Osaka University, Kanazawa University, Hamamatsu University School of Medicine, Chiba University, and University of Fukui, Osaka Japan. [14]Division of Bioscience, Institute for Datability Science, Osaka University, Osaka, Japan. [15]Transdimensional Life Imaging Division, Institute for Open and Transdisciplinary Research Initiatives, Osaka University, Osaka, Japan. [16]Department of Molecular Pharmaceutical Sciences, Graduate School of Medicine, Osaka University, Osaka, Japan.
*Corresponding author. Email: kasai@phs.osaka-u.ac.jp (A.K.); hasimoto@phs.osaka-u.ac.jp (H.H.)
†These authors contributed equally to this work.

that CLA neuronal activation strongly contributed to the discrimination of stressed brains after exposure to acute stressors. CLA neurons received inputs from stress-activated neurons in cortical and subcortical areas, including from the anterior BLA. Chemogenetic activation of the stress-responsive CLA neuronal ensemble and optogenetic terminal photostimulation of stress-responsive BLA neurons in the CLA reproduced anxiety-related behaviors. Conversely, silencing of the CLA neuronal ensemble attenuated anxiety-related behaviors induced by acute social defeat stress (DS) and increased resistance to chronic DS. These results demonstrate that the neuronal ensemble in the CLA serves as a hub for cortico-subcortical communication to control anxiety-related behaviors and thus bidirectionally controls stress-induced emotional responses. This suggests that inactivation of the CLA can be a preventative measure for mitigating stress susceptibility.

RESULTS

CLA activity is a shared trait in stress models

DS and RS are well-known animal models of psychological stress (*16*, *17*). Brain-wide immediate early gene mapping of neuronal activation and unbiased classification of the activation patterns after exposure to these stressors are particularly useful for identifying central stress circuits. We therefore investigated brain-wide neuronal activation after exposure to either of the two stressors in Arc-dVenus reporter mice (*15*). Using our recently developed high-speed imaging system FAST (*12*, *13*), we acquired subcellular-resolution whole-brain images from Arc-dVenus mice subjected to DS or RS and age-matched Arc-dVenus control mice single-housed in their home cages (Fig. 1, A to C). Three-dimensional reconstructed brain images were parcellated into 22 brain regions based on morphological characteristics, and dVenus-positive cells in each region were automatically counted by particle shape analysis (fig. S1, A to E). A comparison of DS- and RS-induced neuronal activation in each region revealed significant changes in the *z* score value of the number of dVenus-positive cells (fig. S1F), including the visual area, ectorhinal area, prelimbic area, nucleus accumbens, CLA, and BLA (Fig. 1D). The fold change of the sample proportion of dVenus-positive cells in each region of RS and DS groups relative to that of home-cage groups was large in the CLA and BLA (fig. S1G). The means ± SEM of the total numbers of dVenus-positive cells were 48.2 ± 16.1 (home cage), 654 ± 385 (RS), and 274 ± 88 (DS). Pearson correlation coefficients within each group (home-cage control mice and RS- and DS-exposed mice; fig. S1H) and their differences revealed a prominent increase in interregional correlations between neurons in the CLA, infralimbic area, and nucleus accumbens in both the DS- and RS-exposed mice (Fig. 1E). This indicates that when the CLA, infralimbic area, or nucleus accumbens is activated, most other brain regions are concomitantly activated upon induction of DS or RS.

To identify the brain regions whose activities are responsive to the two stressors in an unbiased manner, we analyzed the number of dVenus-positive cells in 22 brain regions using a support vector machine, which is a supervised learning model. The scatterplot of the absolute values of the coefficients of the brain regions examined indicated that the CLA, BLA, and visual area predominantly contributed to discrimination between either DS or RS and home-cage control mice (Fig. 1F), among which the CLA showed the strongest contribution to the discrimination of both stress models. The linear support vector classifier faces a potential overfitting issue when used with high-dimension and small–sample size data; to enhance the robustness of the classification analysis, we additionally performed logistic regression with the least absolute shrinkage and selection operator (LASSO), an L1 regularization, which is widely used for dimension reduction and variable selection. The LASSO also showed that the CLA is a common brain area that contributes to discrimination between stressed and home-cage brains (fig. S1I).

DREADD manipulation of stress-responsive CLA ensemble controls anxiety-related behaviors

Because the CLA has a relatively long anteroposterior axis (approximately +1.8 to −1.0 mm across the bregma; fig. S2A), we examined the spatial distribution of dVenus-positive neurons in the CLA after exposure to the stressors to narrow down the region of the CLA that would most contribute to stress responses. The number of dVenus-positive cells was significantly increased in the anterior part of the CLA (approximately +1.52 to +0.96 mm anterior to the bregma) by both stressors (fig. S2, B to H).

To manipulate stress-responsive neurons in the anterior part of the CLA, we first performed molecular characterization of the stress-activated dVenus-positive cells in the anterior part of the CLA (fig. S3; see detailed results and methods in the Supplementary Materials). We revealed that dVenus-positive cells expressed high levels of the excitatory neuron marker *Camk2a* and the CLA markers *Nr4a2*, *Gng2*, and *Gnb4* (*18*–*20*), while the levels of the inhibitory interneuron marker *Pvalb* (*21*) and the insular neuron marker *Crym* (*18*) ranged from low to none (fig. S3F). Immunohistochemistry confirmed that dVenus-positive neurons expressed calcium/calmodulin-dependent protein kinase II α (CaMKIIα) and nuclear receptor subfamily 4 group A member 2 (NR4A2, also known as nur related protein-1, NURR1), but not parvalbumin (fig. S3, G to I).

To explore the role of stress-responsive CLA ensemble in behavioral output, we examined whether chemogenetic designer receptors exclusively activated by designer drugs (DREADD) activation of the stress-responsive CLA excitatory neurons mediates anxiety-related behaviors (Fig. 2). Targeted recombination in active populations (TRAP2) mice (also called $FOS^{2A\text{-}iCreERT2/+}$ mice) (*22*) that were injected with adeno-associated virus (AAV)-CaMKIIα-double-floxed invered open reading frame (DIO)-human M3 muscarinic cholinergic Gq-coupled DREADD (hM3Dq)-mCherry into the CLA and that were exposed to a single session of DS in the presence of tamoxifen (TAM) were administered clozapine-*N*-oxide (CNO) or vehicle and also subjected to behavioral tests (Fig. 2A). In the open-field test, CNO-treated mice spent significantly less time in the anxiogenic center zone, with no significant changes in total locomotor activity, compared to vehicle-treated mice (Fig. 2, B to D). In the elevated plus maze test, CNO-treated mice also displayed a significant decrease in time spent in the anxiogenic open arms, but there was no significant change in the total distance traveled (Fig. 2, E to G). These results showed increased anxiety levels in CNO-treated mice expressing hM3Dq-mCherry.

Next, to test whether chemogenetic silencing of stress-responsive CLA neurons suppresses stress-induced anxiety-related behaviors, we used the inhibitory human M4 muscarinic cholinergic Gi-coupled DREADD (hM4Di) approach (Fig. 3). In this study, the mice were subjected to DS twice. The first DS is to induce stress-mediated targeted recombination in activated neural populations 1 week after AAV injection. The second DS is for behavioral assessment of anxiety behavior, which was applied immediately before the open-field

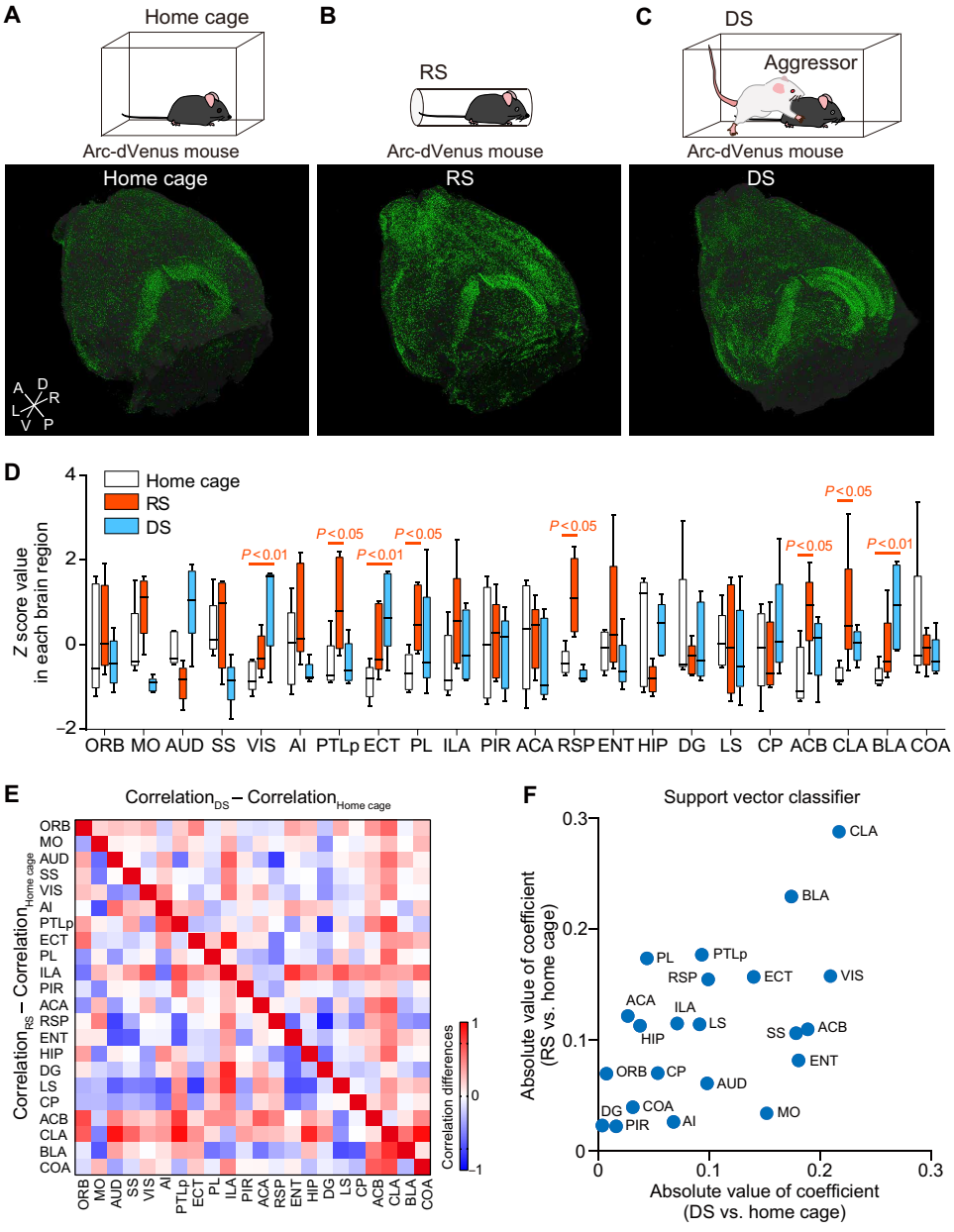

Fig. 1. Brain-wide activation mapping in the acute stress models. (**A** to **C**) Representative whole-brain images of Arc-dVenus mice housed in a home cage (A) or subjected to restraint stress (RS, B) for 30 min or social defeat stress (DS, C) for 10 min. A, anterior; P, posterior; D, dorsal; V, ventral; L, left; and R, right. (**D**) The number of dVenus-positive cells was counted in parcellated brain images of stressed and home-cage mice ($n = 5$ in each group). Box-whisker plot (center, median; box, 25th to 75th percentiles; whiskers, minimum to maximum) shows z-score values of the numbers of dVenus-positive cells in each brain region in RS (orange), DS (blue), and home-cage (white) mice. Two-way ANOVA: brain region, $F(21, 264) < 0.0001$, $P > 0.999$; stress, $F(2, 264) = 7.87$, $P < 0.001$; interaction, $F(42, 264) = 2.71$, $P < 0.001$. (**E**) A correlation matrix showing the difference in interregional activity correlations between home-cage and RS (lower left) or DS (upper right) mice. Red denotes strong positive and blue denotes strong negative correlations. (**F**) Absolute values of coefficients of brain regions are plotted in two classifications (RS versus home cage; DS versus home cage). The coefficients were determined by a linear support vector classifier. Abbreviations for brain areas are shown in table S1.

test. We compared the effects of CNO on stress-induced anxiety-related behaviors of mice expressing the DREADD hM4Di receptor. TRAP2 mice that were injected with AAV-CaMKIIα-DIO-hM4Di-mCherry into the CLA and exposed to a single session of DS in the presence of TAM were administered CNO or vehicle and then subjected to the open-field test (Fig. 3A). Vehicle-treated mice expressing hM4Di-mCherry exhibited a significant decrease in total locomotor activity and time spent in the center zone of the open field after exposure to the second DS (Fig. 3, B and C). This observation was in accord with the previous study showing that acute DS reduced locomotor activity, increased anxiety, and diminished exploratory behaviors (*23*). On the other hand, CNO-treated mice expressing hM4Di-mCherry exhibited a significant increase in the total distance traveled and the ratio of distance traveled in the center zone to total distance traveled during the open-field test after exposure to the second DS compared to vehicle-treated mice expressing hM4Di-mCherry (Fig. 3, B and C).

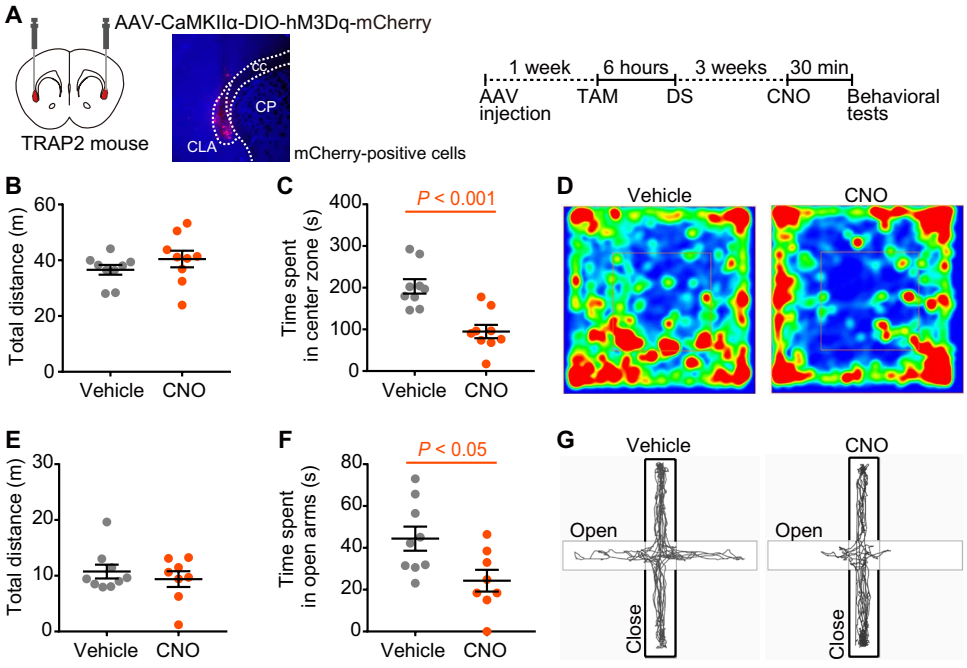

Fig. 2. Chemogenetic activation of the stress-responsive CLA neuronal ensemble reproduces anxiety-related behaviors. (**A**) A schematic of the bilateral injection of the AAV vector (AAV-CaMKIIα-DIO-hM3Dq-mCherry) into TRAP2 mouse and timeline of the experiments for stress-mediated targeted recombination in activated neural populations and behavioral tests. Red areas show the CLA. A representative image shows mCherry-positive cells in the CLA. CP, caudate putamen; cc, corpus callosum; TAM, tamoxifen; DS, social defeat stress; CNO, clozapine-*N*-oxide. (**B** and **C**) Total distance traveled (B) and time spent in the center zone (C) during the open-field test in mice treated with CNO (orange circles; $n = 9$) and vehicle (gray circles; $n = 9$). (**D**) Representative heatmaps showing the position of a mouse treated with vehicle (left) and CNO (right) in the open-field area. Red, more time; blue, less time. (**E** and **F**) Total distance traveled (E) and time spent in the open arms (F) during the elevated plus maze test in mice treated with CNO (orange circles; $n = 8$) and vehicle (gray circles; $n = 9$). (**G**) Representative tracks of a mouse treated with vehicle (left) and CNO (right). Data are the means ± SEM. Statistical analysis was performed using unpaired *t* test.

Since back-conversion of CNO to clozapine may have off-target effects in anxiety-related behaviors (*24*), we used "non-DREADD" control mice that do not express DREADD, which serve as a negative control. Mice expressing hM3Dq-mCherry or mCherry in stress-responsive CLA neurons using a viral-based TRAP approach were administered CNO. After behavioral testing, the behaviors were compared between the two mouse groups (fig. S4, A and B). In the open-field test, CNO-treated mice expressing hM3Dq-mCherry spent significantly less time in the center, with no changes in total locomotor activity, compared to CNO-treated control mice expressing mCherry (fig. S4, C to E). In the elevated plus maze test, CNO-treated and hM3Dq-mCherry–expressing mice also displayed a significant decrease in the time spent in the open arms, but there was no significant change in the total distance traveled (fig. S4, F to H). In addition, we examined anxiety-related behaviors immediately after a single session of DS in CNO-treated mice expressing mCherry and hM4Di-mCherry using a viral-based TRAP approach (fig. S4, I to N). In the open-field test, CNO-treated mice expressing hM4Di-mCherry spent significantly more time in the center zone, with no changes in total locomotor activity, compared to CNO-treated control mice expressing mCherry (fig. S4, I to K). In the elevated plus maze test, CNO-treated mice expressing hM4Di-mCherry also displayed a significant increase in time spent in the open arms, but there was no significant change in the total distance traveled (fig. S4, L to N).

The CLA has reciprocal connections to the medial prefrontal cortex (mPFC) and BLA (*18*, *25*–*27*). Amygdala activation by stressors increases noradrenaline and dopamine levels in the PFC through the stress pathway in the brainstem (*27*–*29*). Even mild acute stress can cause a rapid loss of the PFC functions (*27*). Therefore, we addressed whether manipulation of CLA excitatory neurons regulates anxiety-related behaviors via the catecholamine pathways by examining the changes of catecholamine levels in the mPFC using microdialysis (fig. S5, A to C) and the effects of catecholamine signaling inhibition on anxiety-related behaviors induced by the activation of stress-responsive CLA neurons (fig. S5, D to F). CNO treatment at time 0 during microdialysis significantly increased extracellular levels of both dopamine and noradrenaline in the mPFC in mice expressing hM3Dq-mCherry in the CLA but not in control mice expressing mCherry (fig. S5, B and C). Anxiety-related behaviors induced by chemogenetic reactivation of the stress-responsive CLA ensemble were significantly suppressed by pretreatment with either the dopamine D2 receptor antagonist raclopride or the β-adrenergic receptor antagonist propranolol (fig. S5, D to F). In contrast, pretreatment with the dopamine D1 receptor antagonist SCH39166 or the α1-adrenergic receptor antagonist prazosin showed no effect on anxiety-related behaviors (fig. S5, D to F). In control mice expressing hM3Dq-mCherry without CNO treatment, raclopride and propranolol did not change the total distance traveled or time spent in the open arms in the elevated plus maze test compared to the vehicle-treated control group (fig. S5, G and H), indicating that these antagonists, at least at the dose tested, did not affect total locomotor activity and basal anxiety-related behaviors. These results suggest that catecholamine signals

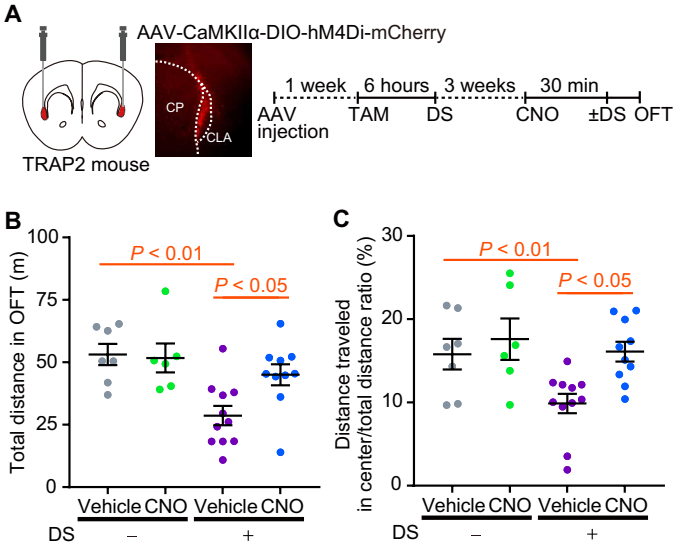

Fig. 3. Chemogenetic silencing of the stress-responsive CLA neuronal ensemble suppresses stress-induced anxiety-related behaviors. (**A**) A schematic of the bilateral injection of the AAV vector (AAV-CaMKIIα-DIO-hM4Di-mCherry) into TRAP2 mouse and timeline of the experiments for stress-mediated targeted recombination in activated neural populations and behavioral test. Red areas show the CLA. A representative image shows mCherry-positive cells in the injection site. CP, caudate putamen. TAM, tamoxifen; DS, social defeat stress; OFT, open-field test. (**B** and **C**) Total distance traveled (B) and the ratio of distance traveled in the center zone to total distance traveled (distance traveled in the center/total distance ratio) (C) during the open-field test in CNO- and vehicle-treated mice with or without exposure to the second DS (gray circles, vehicle treatment without DS, $n = 7$; green circles, CNO treatment without DS, $n = 6$; purple circles, vehicle treatment with DS, $n = 11$; blue circles, CNO treatment with DS; $n = 10$). Data are the means ± SEM. Statistical analysis was performed using two-way ANOVA, followed by Bonferroni multiple comparisons test: stress, $F(1, 30) = 11.64$, $P = 0.0019$; treatment, $F(1, 30) = 2.68$, $P = 0.112$; interaction, $F(1, 30) = 3.77$, $P = 0.062$ (B); stress, $F(1, 30) = 5.46$, $P = 0.026$; treatment, $F(1, 30) = 6.41$, $P = 0.017$; interaction, $F(1, 30) = 1.94$, $P = 0.17$ (C).

are involved in the underlying behavioral changes by the stress-responsive CLA ensemble.

CLA neurons receive inputs from stress-responsive BLA and cortical neurons

To identify neural connections of stress-activated neurons to the anterior parts of the CLA, we performed Cre-dependent retrograde tracing with an AAV and TRAP2 mice. After infection with red fluorescent protein mCherry-expressing and Cre-dependent enhanced green fluorescent protein (EGFP)–expressing retrograde AAV vectors (AAVrg) into the CLA of a TRAP2 mouse, the TRAP2 mouse was subjected to a single session of DS in the presence of TAM to label stress-activated neurons projecting to the CLA with EGFP (fig. S6A). We found EGFP-positive neurons projecting to the CLA in various brain areas, including the anterior olfactory, agranular insular, prelimbic/infralimbic areas, anterior cingulate area (ACA), BLA, piriform, ectorhinal, and entorhinal areas (fig. S6, B to K). Compared with mCherry-labeled neurons projecting to the CLA in TRAP2 mice, approximately 20% of CLA-projecting neurons in the BLA were stress-responsive EGFP-labeled neurons (fig. S6, L and M). This was the highest ratio among the brain areas examined. These results suggest that stress-responsive CLA-projecting neurons are abundant in the BLA among brain regions such as the mPFC and ACA (*25*).

The anterior and posterior parts of the BLA have been shown to differ functionally and genetically and to elicit emotionally opposing effects (*30*). Therefore, we next compared the anteroposterior distribution of mCherry-labeled BLA neurons projecting to the CLA with that of EGFP-labeled stress-responsive BLA neurons projecting to the CLA (fig. S7). The mCherry-labeled BLA neurons were detected throughout the anterior and posterior parts of the BLA (approximately −0.5 to −2.0 mm from the bregma). In contrast, EGFP-labeled stress-responsive BLA neurons projecting to the CLA were mainly detected in the anterior part of the BLA (−0.5 to −1.6 mm from the bregma) (fig. S7).

Optogenetic stimulation of stress-responsive BLA terminals in the CLA temporally controls anxiety-related behaviors

Since CLA neurons received stress-responsive BLA inputs (fig. S6), we examined whether activation of stress-responsive BLA neuronal terminals in the CLA is sufficient to induce an increase in anxiety-related behaviors. TRAP2 mice that were bilaterally injected with AAV-CaMKIIα-DIO-Chronos-EGFP or AAV-CaMKIIα-DIO-EGFP into the BLA and bilaterally implanted with optical fiber over the CLA were exposed to a single session of DS in the presence of TAM and then subjected to a real-time place preference test and an open-field test (fig. S8). In the real-time place preference test, photostimulation of stress-responsive BLA terminals in the CLA did not change locomotor activity but significantly decreased time spent in the photostimulation zone compared to the nonphotostimulation zone in mice expressing Chronos-EGFP (fig. S8, B to D). The open-field test for 9 min with 3-min OFF-ON-OFF epochs showed that mice expressing Chronos-EGFP displayed a decrease in time spent in the center zone upon illumination during the ON epoch relative to mice expressing EGFP controls without affecting locomotion during the ON epoch relative to the baseline OFF epoch (fig. S8, E and F).

Silencing of stress-responsive CLA neurons attenuates depression-like behavior

Last, we addressed whether chemogenetic silencing of the stress-responsive CLA neuronal ensemble tagged during DS affects the emergence of depression-like behavior using a chronic DS model of depression (Fig. 4). TRAP2 mice that expressed hM4Di-mCherry or mCherry in the CLA and underwent a single session of DS in the presence of TAM were administered CNO 30 min before DS for 10 min every day for 10 days and subjected to social interaction, elevated plus maze, forced swimming, and sucrose preference tests (Fig. 4A). Compared with CNO-treated control mice expressing mCherry, mice expressing hM4Di-mCherry showed a significantly attenuated reduction in the interaction ratio during the social interaction test (Fig. 4, B to F) and an increased sucrose preference (Fig. 4G). The time spent in the open arms in the elevated plus maze test and immobility time in the forced swimming test did not significantly differ between mice that expressed hM4Di-mCherry and those that expressed mCherry (Fig. 4, H and I). These results suggest that inactivation of stress-responsive CLA neurons can serve as a partially preventative measure for the emergence of depression-like behavior.

DISCUSSION

The present study demonstrates that the CLA is crucially involved in stress-induced neurobehavioral changes, in which manipulation

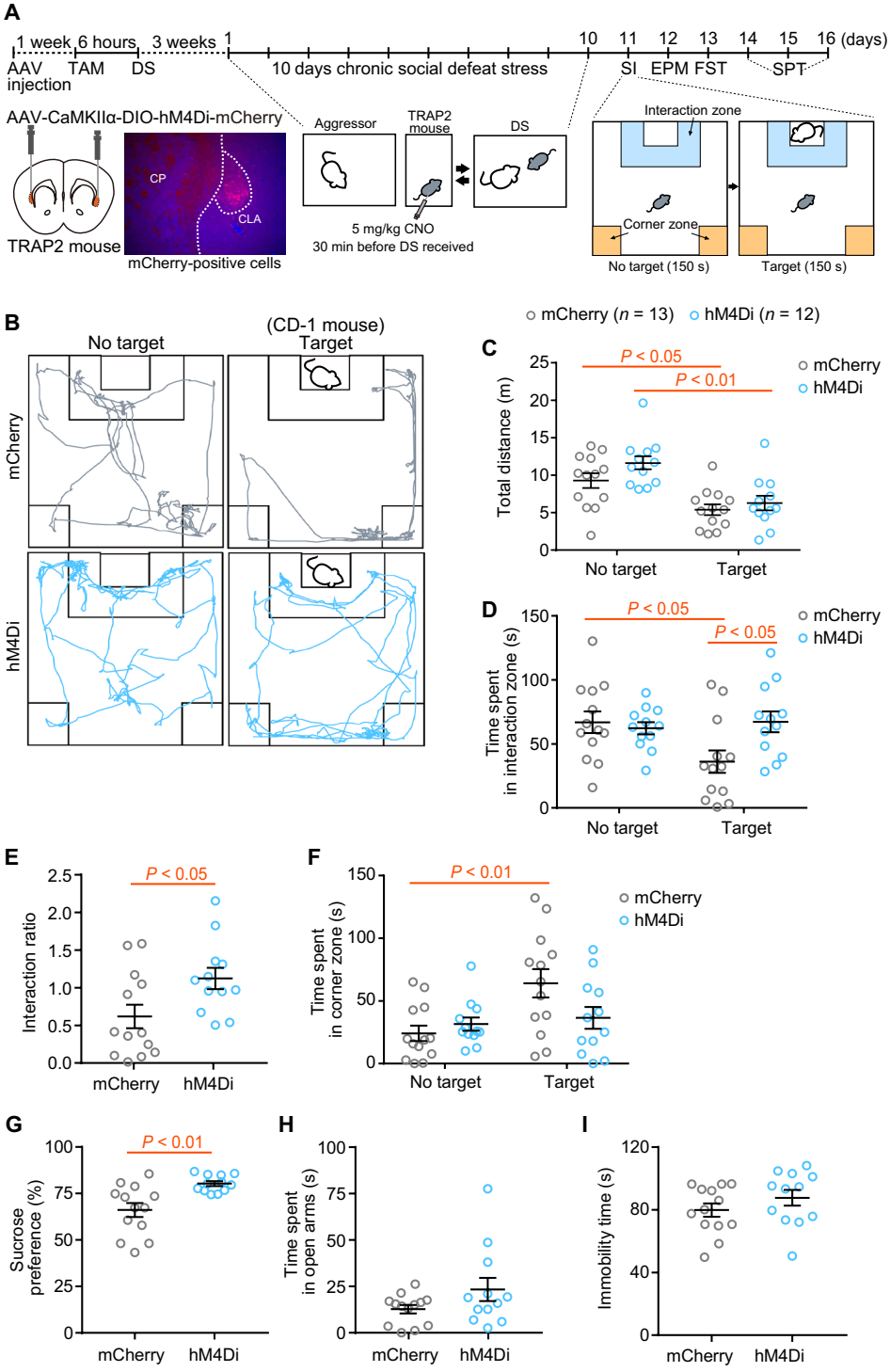

Fig. 4. Chemogenetic inhibition of the stress-responsive CLA neuronal ensemble partly protects against stress-related behaviors. (**A**) Schematic of experimental design. A representative image shows mCherry-positive cells in the CLA. SI, social interaction test; EPM, elevated plus maze test; FST, forced swim test; SPT, sucrose preference test. (**B**) Representative tracks of a mouse expressing hM4Di-mCherry and mCherry in the presence or absence of a target mouse. (**C** to **I**) Total distance traveled (C), time spent in the interaction zone (D), interaction ratio (E), and time spent in the corner zone (F) during the SI, sucrose preference in the SPT (G), time spent in the open arms during the EPM (H), and immobility time in the FST (I) in mice expressing hM4Di-mCherry (blue circles) and mCherry (gray circles). Statistical analysis was performed as follows: total distance traveled (C), two-way ANOVA: target, $F(1,46) = 25.8$, $P < 0.0001$; DREADD, $F(1,46) = 3.12$, $P = 0.084$; interaction, $F(1,46) = 0.637$, $P = 0.43$; time spent in the interaction zone (D), two-way ANOVA: target, $F(1,46) = 2.72$, $P = 0.11$; DREADD, $F(1,46) = 2.88$, $P = 0.096$; interaction, $F(1,46) = 5.27$, $P = 0.026$; interaction ratio (E), unpaired t test; time spent in the corner zone (F), two-way ANOVA: target, $F(1,46) = 7.34$, $P = 0.0094$; DREADD, $F(1,46) = 1.49$, $P = 0.23$; interaction, $F(1,46) = 4.47$, $P = 0.040$; sucrose preference (G), unpaired t test; time spent in the open arms (H), Welch's t test, $P = 0.13$; immobility time (I), unpaired t test, $P = 0.24$. As a post hoc analysis, Bonferroni multiple comparisons test was conducted (C, D, and F). Data are the means ± SEM.

of the stress-responsive neuronal ensemble bidirectionally controls anxiety-related behavior, as activation augments anxiety-related behaviors and inactivation normalizes them. Stress-responsive neurons that projected to the CLA were widely distributed in the brain. In particular, inputs from the BLA were prominent. Optogenetic activation of the BLA inputs to the CLA increased anxiety-related behaviors. In addition, chemogenetic activation of CLA neurons increased dopamine and noradrenaline release in the mPFC, and blockade of dopamine and noradrenaline signaling attenuated anxiety-related behaviors, implying that activation of the CLA ensemble could reproduce catecholamine responses underlying acute stress responses. Furthermore, chemogenetic silencing of the CLA ensemble improved chronic DS–induced reduction of social interaction and anhedonia and, thus, increased resilience. These results clearly demonstrate that the CLA is implicated in the brain stress circuitry and that it bidirectionally controls stress-induced emotional responses.

Although accumulating evidence has reported CLA neuronal activation by aversive stimuli in humans (*31*, *32*) and rodents from other groups (*33*) and our group (*12*), only a few studies have investigated the function of the CLA in emotional control. The CLA has a very thin structure (*34*), and in our study, only 273.6 ± 88.2 and 654 ± 385 CLA neurons were activated in RS- and DS-exposed Arc-dVenus mice, respectively, while 48.2 ± 16.1 (n = 5) neurons were activated in control mice. As the total number of Hoechst 33258–stained cell nuclei in the CLA was 139,955 ± 7,897 (n = 3) (*12*), the number of additionally activated CLA neurons in the RS- and DS-exposed mice above that in the control mice amounted to 0.16 and 0.43% of all cells, respectively. In the present study, we quantitatively compared the number of activated neurons in mice that underwent RS and DS and subjected the data to support vector machine and LASSO-supervised classification algorithms. Both indicated that the CLA strongly contributed to the discrimination between the two stress models and home-cage control mice. In addition, interregional correlations of neuronal activation were remarkably increased between the CLA and the other regions in both stress models (Fig. 1E). We therefore hypothesized that the CLA played a key role in the control of stress-induced neurobehavioral changes. The quantitative classification approach of brain activation mapping was very useful for identifying important elements, especially when they are small regions composed of a small number of cells.

It is well known that the BLA is an integrative hub for regulating affective behaviors (*8*). The broadcasting of emotional signals from the BLA to larger brain networks likely plays an important role in state-dependent regulation and modulation of affective states and behaviors; however, the underlying downstream pathways remain elusive (*9*). The functional genetic labeling conducted in this study showed that the anterior part of the CLA received input from stress-responsive BLA neurons (fig. S6) and that photostimulation of stress-responsive BLA terminals in the CLA induced anxiety-related behaviors (fig. S8). In addition, the CLA and BLA predominantly contributed to the discrimination of brain states after exposure to stressors (Fig. 1). Imaging studies in the human amygdala/CLA region (the CLA extending into the amygdala) have shown that aversive stimuli activated this region (*35*, *36*). This observation also suggests that the CLA ensemble is functionally and anatomically connected to the BLA and thereby modulates emotional processes. The anterior and posterior parts of the BLA have been shown to differ functionally and genetically and to elicit emotionally opposing effects. Optogenetic activation of the anterior BLA neurons evoked negative emotional behavior (disrupting reward-seeking behaviors), while that of the posterior BLA neurons induced positive effects (*30*). This suggests that the CLA ensemble plays a key role downstream of the anterior BLA, and thus, activation (or inactivation) of this pathway can evoke (or attenuate) anxiety-related behaviors.

The present studies indicate that catecholamine signalings were involved in anxiety-related behaviors due to activation of stress-responsive CLA ensemble (fig. S5), although CLA projections are rarely innervated directly to the locus coeruleus (LC) and ventral tegmental area (VTA) (*18*, *25*, *26*), which are respectively the main sources of noradrenaline and dopamine in the brain. Stress triggers the tonic neuronal activity of LC neurons through corticotropin-releasing hormone neurons in the central amygdala, leading to anxiety-related behaviors (*4*). The main projection of the CLA extends to the cortices, such as the frontal cortex, and also to the BLA (*25*, *26*). Therefore, although further experiments are needed, a stress-responsive CLA ensemble may affect LC activity via the BLA-central amygdala circuit. In addition, CLA-to-cortical projections inhibit the prefrontal cortex's activity (*26*, *37*). The PFC also has direct and indirect connections to the LC, VTA, and amygdala and can regulate its own catecholamine inputs (*27*). Under psychological stress conditions, stress-responsive CLA ensemble may impair this PFC regulation of catecholamine and/or weaken the BLA inhibition from mPFC neurons (*38*–*40*).

Silencing of the CLA ensemble during DS suppressed subsequent anxiety-related and depression-like behaviors (Figs. 3 and 4 and fig. S4). As activation of the CLA ensemble caused anxiety-related behaviors (Fig. 2), silencing of the CLA ensemble may reduce anxiety in mice during DS, lowering the experience of social defeat. This may have resulted in reduced anxiety-related behaviors immediately after DS in subsequent behavioral tests.

Accumulating evidence indicates that the CLA may be involved in the salience network in the rodent and human brain (*41*–*44*). Aversive salience, the aversive form of motivational salience, enhances vigilance causing consequent anxiogenic responses and avoidance behavior. Salient sensory stimuli increase dopamine neuron activity and dopamine release (*45*). The catecholamine system in the PFC is involved in motivational salience (*46*). We found that CLA ensemble activated by aversive stimuli increased the dopamine and noradrenaline levels in the PFC, followed by the emergence of anxiety-related behaviors (fig. S5). These data imply that CLA activation may be involved in salient information processing in the open arms of the elevated plus maze, leading to enhanced vigilance. On the other hand, Terem *et al.* (*43*) recently found that the CLA-to-frontal cortical circuit directs attention to salient incentive cues through dopamine D1 signal. The mPFC-projecting VTA dopamine neurons are activated by aversive stimuli such as DS, whereas the nucleus accumbens (ACB)-projecting VTA dopamine neurons are activated by rewarding stimuli such as cocaine (*47*, *48*). Because D2 antagonist, but not D1 antagonist, blocked CLA activation–induced anxiety-related behaviors, the difference in the role of the CLA neurons in aversive and incentive salience may be due to the difference in the type of DA neurons that respond to different types of stimuli.

Excessive or repeated stress can lead to psychiatric disorders, e.g., posttraumatic stress disorder and depression. In the present study, we showed that chemogenetic silencing of the CLA neuronal ensemble attenuated the depression-like behavior caused by chronic

DS (Fig. 4). In this study, the impairment in social interaction and anhedonia (reduced sucrose preference) was significantly normalized; however, results in the elevated plus maze test and forced swimming tests were not altered by CLA inhibition. These observations are in agreement with the results from previous reports (*49*). Although chronic DS produces two operationally segregated groups, "susceptible" and "resilient," the former developing social avoidance and anhedonia, both groups show increased anxiety-related behaviors in the elevated plus maze and a normal level of immobility in the forced swimming test (*49*). These results suggest that inactivation of stress-responsive CLA neurons can serve as at least a partially preventative measure for the emergence of depression-like behavior and, moreover, for stress susceptibility to increase resilience to emotional stress. Future studies are warranted to examine whether CLA neuronal activity can be a therapeutic target, and whether it can be a potential biomarker for stress-related disorders, as well as to identify molecular targets to control neuropsychiatric diseases.

Limitations of the study

We obtained relatively exclusive CLA infection following DS-induced Cre-limited expression using either TRAP2 mice with AAV vectors or viral-based TRAP technique and identified the important role of the CLA in stress-induced anxiety responses. However, several experimental limitations of the study are worth noting. First, with the techniques used, which do not use the CLA's molecular markers but are controlled by TRAP2 mice and AAV vectors, it is difficult to control the leakage into the surrounding areas, especially the dorsal endopiriform nucleus, completely. For this reason, the possibility of involvement of stress-responsive neurons adjacent to the CLA in the regulation of anxiety responses cannot be completely ruled out. Second, because of variations of virus injections, the number of manipulated neurons would vary among experimental animals. These issues should be addressed using transgenic animal tools, as described in previous studies (*26*, *43*, *50*), to ensure the specificity of the manipulation to the CLA or to reduce the variance across the experiments. Last, there is the lack of a reference for CLA neurons captured in a novel environment in the absence of stress. As the CLA is reactive to a novel environment (*51*), random populations of the CLA neurons captured by exposure to a novel environment in the absence of stress may support the same functional results as seen in this study. Therefore, the results of our manipulations may need to consider the effect of a novel environment-responsive DS neurons in addition to DS-responsive CLA neurons.

MATERIALS AND METHODS

Animals

All animal care and handling procedures were approved by the Animal Care and Use Committee of Osaka University (approval numbers 28-1-12 and R02-8-2). All efforts were made to minimize the number of animals used. The following adult (7 to 14 weeks of age) male mice were used throughout the study. Arc-dVenus reporter mice (*15*), which express the destabilized fluorescent protein dVenus driven by the *Arc* gene promoter on a C57BL/6J background, were used for activity mapping and single-cell RNA sequencing analysis; C57BL/6J wild-type mice (SLC, Shizuoka, Japan) were used for behavioral and microdialysis studies; CD1 wild-type mice (SLC) were used for behavioral study; and $FOS^{2A\text{-}iCreER}$ knock-in mice (TRAP2; JAX stock no. 030323, The Jackson Laboratory, Bar Harbor, ME) (*22*), which express TAM-dependent iCreER recombinase driven by the *cFos* gene promoter, were used for retrograde tracing, behavioral, and optogenetic studies. Mice were maintained in group housing (three to six mice per cage) except for singly housed treated mice. They were kept on a 12-hour light-dark cycle (lights on at 8:00 a.m.) with controlled room temperature and water and food (CMF, Oriental Yeast, Osaka, Japan) available ad libitum.

DS and RS models

Mice were housed alone at least 1 week before exposure to stressors. For DS, CD-1 mice were prescreened for aggressive behaviors toward a naïve C57BL/6J mouse as described previously (*52*) with minor modifications. When the attack latencies are shorter than 60 s, and two or more attacks are within 3 min on at least two of three consecutive days, that CD-1 mouse was used as an aggressor for DS. Test mice were exposed to a resident aggressor CD-1 mouse for 10 min and returned to the home cage. Chronically defeated mice were exposed to DS for 10 min per day for 10 consecutive days. For RS, test mice were placed for 30 min in a restrainer fashioned from a 50-ml polypropylene tube with holes at the tips and lateral sides for unrestricted breathing as described previously (*12*).

Tissue preparation

Mice were deeply anesthetized via an intraperitoneal injection of a mixture containing medetomidine (3 mg/kg; Nippon Zenyaku Kogyo, Fukushima, Japan), midazolam (4 mg/kg; Sandoz Pharma, Basel, Switzerland), and butorphanol (5 mg/kg; Meiji Seika Pharma, Tokyo, Japan) and were transcardially perfused with saline followed by 4% paraformaldehyde (Nacalai Tesque, Kyoto, Japan) dissolved in phosphate-buffered saline [PBS; 137 mM NaCl, 8.1 mM $Na_2HPO_4/12H_2O$, 2.7 mM KCl, and 1.47 mM KH_2PO_4 (pH 7.4)]. Brains were excised and immersed in 4% paraformaldehyde in PBS until use.

Whole-brain imaging and brain-wide activation mapping

For serial whole-brain imaging, our recently developed high-speed serial-sectioning imaging system, FAST, was used, and the imaging was conducted as described previously (*12*, *13*, *53*). Briefly, brains were fixed with 4% paraformaldehyde in PBS and embedded in 3.5 to 4% agarose gel (Nacalai Tesque) dissolved in PBS, and optical brain section images were acquired as a mosaic of fields of view with 20% overlap in the *x-y* plane and 30-μm overlap in the *z* direction with a resolution of 1.0 μm in the *x-y* plane and 5.0 μm in the *z* direction. The *x-y* plane section images were then reconstructed from the field-of-view tiles by overlapping alignment of consecutive sections using the C++ program TileTiff (Neuro Programming Research Co., Toyonaka, Japan) (*12*) and an in-house all-in-one stitching program, FASTitcher, written in Python 3.6 (*13*). The resulting section images were aligned in the *z* direction by stitching with the *z* direction overlap. Each dVenus-positive cell body was detected by three-dimensional particle recognition using TRI/FCS-NUC64 software (R.10.00.04.3-3-H-64; Ratoc System Engineering, Tokyo, Japan), and the spatial coordinates of all dVenus-positive cells were obtained. To determine the cell numbers, 22 brain areas (except for the lateral septum, the 21 regions were segmented separately by hemisphere and then combined; fig. S1) were manually parcellated every 50 to 100 μm of the stitched images and automatically complemented in the other images using TRI/FCS-NUC64 software.

Machine learning classifiers

The number of dVenus-positive cells of each region was normalized by dividing by the total number of dVenus-positive cells in a mouse and then transformed into *z*-score data (average 0 and variance 1 for each region). Support vector classification for the normalized datasets (DS or RS versus control) was implemented using the scikit-learn function svm (*54*) with the linear kernel of the Python library. GridSearchCV in the scikit-learn library was used for hyperparameter optimization. Logistic regression with LASSO (L1-norm regularization) (*55*) was performed for the normalized datasets by the scikit-learn function Logistic Regression of the Python library (*54*).

Spatial distribution analysis of dVenus-positive cells in the CLA

The CLA (approximately spanning from the bregma +1.8 to −1.0 mm anterior/posterior) was equally divided into 10 anterior-posterior parts based on the appropriate number of bins given by Sturges' rule (*56*). Using the spatial coordinates of all dVenus-positive cells in the CLA analyzed by TRI/FCS-NUC64 software, the number of dVenus-positive cells was counted in each bin.

Immunohistochemistry

Tissue blocks containing the CLA were sliced into 50-μm-thick coronal sections using a linear slicer (Pro7N, Dosaka EM, Kyoto, Japan). The sections were then subjected to a conventional free-floating staining technique as described previously (*57*) with minor modifications. Briefly, the sections were blocked with 2% bovine serum albumin (Nacalai Tesque) in tris-buffered saline [50 mM tris HCl, 138 mM NaCl, and 2.7 mM KCl (pH 7.6)] containing 0.3% Triton X-100 (Nacalai Tesque) for 1 hour at room temperature, incubated with mouse anti-CaMKIIα monoclonal antibody (1:50 dilution; catalog number sc-13141, Santa Cruz Biotechnology, Santa Cruz, CA) or mouse anti-parvalbumin monoclonal antibody (1:5000 dilution; catalog number 235, Swant, Bellinzona, Switzerland) overnight at 4°C and then with Alexa 594–conjugated goat anti-mouse immunoglobulin G (IgG) secondary antibody (1:1000 dilution; catalog number A-11005, Life Technologies, Carlsbad, CA) for 1 hour at room temperature. For immunostaining of the CLA marker NR4A2, paraformaldehyde-fixed brains were cryoprotected in 20% sucrose dissolved in PBS for 2 days and sliced into 50-μm-thick coronal sections. The sections were pretreated with HistoVT-One (Nacalai Tesque) at 80°C for 30 min for antigen activation and incubated with mouse anti-Nurr1 monoclonal antibody (1:50 dilution; catalog number sc-376984, Santa Cruz Biotechnology) and then with Alexa 594–conjugated goat anti-mouse IgG secondary antibody (1:1000 dilution).

Generation of AAV transgenes

pAAV-CaMKIIα-double inverted open reading frame (DIO)-hM3Dq-mCherry was produced as described previously (*58*). To construct pAAV-CaMKIIα-DIO-mCherry for use as a control vector, pAAV-CaMKIIα-DIO-hM3Dq-mCherry was digested with BamHI-HF (R3136, New England Biolabs, Ipswich, MA) and BmtI-HF (R3658, New England Biolabs) to delete the hM3Dq sequence and self-ligated with a linker and the DNA Ligation Kit Mighty Mix (Takara Bio, Otsu, Japan).

pAAV-CaMKIIα-DIO-hM4Di-mCherry was produced by exchanging the hM3Dq-mCherry of pAAV-CaMKIIα-DIO-hM3Dq-mCherry with the hM4Di-mCherry from pAAV-hSyn-DIO-hM4Di-mCherry [a gift from B. Roth; Addgene plasmid no. 44362; http://n2t.net/addgene:50475; Research Resource Identifier (RRID): Addgene_44362] using AscI (R0558, New England Biolabs) and NheI-HF (R3131, New England Biolabs) and DNA Ligation Kit Mighty Mix.

For construction of pAAV-Fos-ER^{T2}CreER^{T2}, in which Cre-recombinase is expressed under the control of the Fos minimal promoter and activated in the presence of TAM, a Fos minimal promoter segment cassette from fos-tTA (a gift from M. Mayford; Addgene plasmid no. 34856; http://n2t.net/addgene:34856; RRID: Addgene_34856) (*59*), Cre recombinase fused to a mutant estrogen ligand-binding domain ER^{T2}CreER^{T2} cassette from pCAG-ER^{T2}CreER^{T2} (a gift from C. Cepko; Addgene plasmid no.13777; http://n2t.net/addgene:13777; RRID: Addgene_13777) (*60*), and a fused protein-degradation sequence hCL1–hPEST cassette from pGL4.12[luc2CP] vector (E6671, Promega, Madison, WI) were amplified using Q5 Hot Start High-Fidelity 2× Master Mix (New England Biolabs) and subcloned into MluI-HF (R0198, New England Biolabs)– and BglII (10348767001, Roche, Tokyo, Japan)–digested pAAV-hSyn-DIO-hM4Di-mCherry using an In-Fusion HD cloning kit (Clontech, Mountain View, CA).

To construct pAAV-CaMKIIα-hM3Dq-mCherry, which lacks the DIO sequences, the hM3Dq-mCherry sequence was amplified from pAAV-CaMKIIα-DIO-hM3Dq-mCherry and subcloned in an inverted orientation into AccI (R0161, New England Biolabs)– and EcoRI-HF (R3101, New England Biolabs)–digested pAAV-CaMKIIα-DIO-hM3Dq-mCherry using an In-Fusion HD cloning kit. To construct pAAV-CaMKIIα-mCherry for use as a control vector, pAAV-CaMKIIα-hM3Dq-mCherry was digested with AccI and BamHI-HF to delete the hM3Dq sequence and self-ligated with an adaptor and DNA Ligation Kit Mighty Mix. For construction of pAAV-hSyn-mCherry, mCherry cassette was cut from pAAV-CaMKIIα-mCherry using EcoRI-HF and BamHI-HF and ligated with EcoRI-HF– and BamHI-HF–digested pAAV-hSyn-DIO-hM4Di-mCherry.

For construction of pAAV-CaMKIIα-DIO-Chronos-EGFP, Chronos-EGFP was cut from pAAV-Syn-Chronos-EGFP (a gift from E. Boyden; Addgene plasmid no. 59170; http://n2t.net/addgene:59170; RRID: Addgene_59170) using BsrGI (R0575, New England Biolabs) and BamHI-HF and ligated with BsrGI– and BmtI-HF–digested pAAV-CaMKIIα-DIO-hM3Dq-mCherry in an inverted orientation using a linker and DNA Ligation Kit Mighty Mix. pAAV-CaMKIIα-DIO-EGFP was produced by exchanging the mCherry of pAAV-CaMKIIα-DIO-mCherry with the EGFP from pAAV-hSyn-DIO-EGFP (a gift from B. Roth; Addgene plasmid no. 50457; http://n2t.net/addgene:50457; RRID: Addgene_50457) using MluI-HF, BamHI-HF, and DNA Ligation Kit Mighty Mix.

Virus production and purification

AAV vectors were produced by the helper-free triple transfection procedure as described previously (*61*). Briefly, an AAV transgene was transfected with a pAAV-DJ (Cell Biolabs, San Diego, CA) or rAAV2-retro plasmid (a gift from A. Karpova and D. Schaffer, Addgene plasmid no. 81070; http://n2t.net/addgene:81070; RRID: Addgene_81070) (*62*), which supplies AAV2 replication proteins and AAV-DJ or AAV2-retro capsid proteins (AAVdj or AAVrg, respectively), and with a pHelper plasmid, which supplies the necessary adenovirus gene products required for AAV production, into human embryonic kidney 293T cells using polyethyleneimine (Polyscience Inc., Warrington, PA). After 60 to 72 hours, the transfected cells were suspended in 10 mM tris with 10 mM $MgCl_2$ and 150 mM NaCl (pH 7.6), freeze-thawed three times, and treated with ≥250 U/μl of Benzonase nuclease (Sigma-Aldrich, St Louis, MO) at

37°C for at least 45 min. The suspension was centrifuged at 3000*g* for 15 min at 4°C, and the supernatant was loaded onto an iodixanol step gradient (15, 25, 40, and 58%; Optiprep, Cosmo Bio, Tokyo, Japan) and centrifuged at 278,400*g* for 105 min at 18°C. Concentrated AAV vectors were removed from the 40% iodixanol layer. The AAV was titrated by quantitative real-time polymerase chain reaction using GoTaq qPCR Master Mix (Promega) with linearized genome plasmid as a standard.

Stereotaxic surgery

Mice were anesthetized using 2.5 to 3.5% isoflurane (FUJIFILM Wako Pure Chemical Corp., Osaka, Japan) and placed in a stereotaxic apparatus (David Kopf Instruments, Tujunga, CA; Stoelting, Wood Dale, IL). Microinjection into the CLA (stereotaxic coordinates: +1.5 mm anterior, ± 2.3 mm lateral, and −3.5 mm ventral to the bregma) or the BLA (stereotaxic coordinates: −1.4 mm anterior, ±3.3 mm lateral, and −4.5 mm ventral to the bregma) was performed using a NanoFil Syringe (World Precision Instruments, Sarasota, FL) or a Gastight Syringe (Hamilton, Reno, NV) with a 33-gauge needle and an UltraMicroPumpIII with a Micro4 controller (World Precision Instruments). AAV liquid was deposited at a rate of 100 nl/min. The needle was left in place for 5 min before withdrawal and then slowly removed to avoid backflow. After stereotaxic surgery, the mice received an intraperitoneal injection of buprenorphine (0.1 mg/kg; Otsuka Pharma, Tokyo, Japan) and gentamicin (10 mg/kg; Sigma-Aldrich) and allowed to recover for 1 week.

DREADD expression in the CLA for manipulating neuronal activity

Neuronal activity was specifically manipulated using the DREADD platform as described previously (*63*). Excitatory DREADD hM3Dq was expressed in the CLA by bilateral injection of a mixture of AAVdj-Fos-ER^{T2}CreER^{T2} (8.5×10^{13} particles/ml) plus AAVdj-CaMKIIα-DIO-hM3Dq-mCherry (4.7×10^{12} particles/ml) (50 nl of each AAV, 100 nl total volume per side) or AAVdj-CaMKIIα-hM3Dq-mCherry (4.5×10^{12} particles/ml; 50 nl per side). Inhibitory DREADD hM4Di was expressed in the CLA by bilateral injection of a mixture of AAVdj-Fos-ER^{T2}CreER^{T2} (8.5×10^{13} particles/ml) plus AAVdj-CaMKIIα-DIO-hM4Di-mCherry (4.4×10^{12} particles/ml) (50 nl of each AAV, 100 nl total volume per side) or AAVdj-CaMKIIα-DIO-hM4Di-mCherry (4.4×10^{12} particles/ml; 50 nl per side). As negative controls for Cre-dependent and constitutive CaMKIIα promoter–driven DREADD experiments, a mixture of AAVdj-Fos-ERT2CreERT2 plus AAVdj-CaMKIIα-DIO-mCherry and AAVdj-CaMKIIα-mCherry were injected into the CLA, respectively.

Behavioral experiments were performed at least 3 weeks after genetic labeling. For neuronal activation, mice expressing hM3Dq-mCherry or mCherry (as a control) received an intraperitoneal injection of CNO (1 mg/kg; Cayman Chemical, Ann Arbor, MI) dissolved in saline containing 1% dimethyl sulfoxide (DMSO) 30 min before behavioral tests. For neuronal inhibition, mice expressing hM4Di-mCherry or mCherry (as a control) received an intraperitoneal injection of CNO (5 mg/kg) 30 min before the behavioral tests or exposure to DS.

Behavioral tests

Open-field test

An open-field test was performed in a square box (42 cm width by 42 cm depth by 30 cm height) under 40 to 50 lux light intensity as described previously (*64*) with minor modifications. Each mouse was placed in the center of the open field and was allowed to move freely for 20 min. The activity of the mouse was recorded using a video camera (HC-V600M, Panasonic, Osaka, Japan), and the total locomotor activity (total distance traveled) and distance traveled and time spent in the center area (21 cm by 21 cm square) were analyzed using ANY-maze video-tracking software (version 4.99 m, Stoelting, Wood Dale, IL). The open field was cleaned with 70% ethanol between each trial.

Elevated plus maze test

The elevated plus maze test was performed as described previously (*64*) with minor modifications. The elevated plus maze apparatus (Brain Science Idea, Osaka, Japan), consisting of two open arms (25 cm length by 8 cm width) and two enclosed arms (25 cm length by 8 cm width, surrounded by a 20-cm-high opaque wall), was elevated 50 cm from the ground. Each mouse was placed on the central platform with its head facing one of the closed arms and was allowed to move freely for 5 min under 50 lux light intensity. The activity of the mouse was recorded using a video camera, and the total distance traveled and time spent in the open arms were analyzed using ANY-maze video-tracking software. The maze was cleaned with 70% ethanol between each trial.

Social preference avoidance test

The social interaction test was performed as described previously (*65*). During the first session (no target), for 150 s, the open field contained an empty wire mesh cage (8 cm by 6 cm) located at one end of the field. During the second session (target), for 150 s, the conditions were identical except that a social target animal (an unfamiliar CD1 male mouse) was introduced in the mesh cage. Between these sessions, the experimental mouse was removed from the arena and placed back into its home cage for approximately 1 min. All social interaction testing was conducted under red-light conditions. The performance of the mouse was recorded for approximately 6 min using a video camera, and the time spent by the test mouse in the "interaction zone" (an 8-cm-wide corridor surrounding the mesh cage) and the "corner zone" (9 cm by 9 cm) opposite the location of the mesh cage was analyzed using ANY-maze video-tracking software. The social interaction ratio was calculated as the ratio of the time spent in the interaction zone in the target session to the time spent in the interaction zone in the no-target session. The open field was cleaned with 70% ethanol between each trial.

Forced swim test

The forced swim test was conducted by placing the mice into an individual acrylic cylinder (25 cm height by 19 cm diameter) containing 25° ± 1°C water at a depth of 13 cm, as described previously (*66*). The performance of the mice in the swimming session was recorded for 6 min using a video camera. After the session, the mice were removed from the cylinders, dried with paper towels, and then returned to their home cages. The total time of immobility was measured over the last 2 min of the session by video observation by a trained observer blind to the experimental conditions.

Sucrose preference test

The sucrose preference test was performed as described previously (*67*) with minor modifications. Water bottles in the home cages were replaced with two 50-ml conical tubes with sipper tops filled with water. After habituation for 24 hours, one of the 50-ml conical tubes was filled with a 1% sucrose solution. All tubes were weighed, and the mice were allowed to drink ad libitum for a 24-hour period. The tubes were then reweighed, and the position of the tubes was

interchanged for another 24-hour period of ad libitum drinking. Sucrose preference was calculated as a percentage of the volume of sucrose consumed over the total volume of sucrose and water consumed expressed as a percentage and averaged over 2 days.

Microdialysis

Microdialysis was performed as described previously (*68*) with minor modifications. The mice were anesthetized with medetomidine (0.3 mg/kg), midazolam (4 mg/kg), and butorphanol (5 mg/kg) and stereotaxically implanted with a guide cannula for a dialysis probe (Eicom, Kyoto, Japan) in the mPFC (stereotaxic coordinates: +1.9 mm anterior, −0.5 mm lateral, and −0.8 mm ventral to the bregma). The cannula was cemented in place with dental acrylic, and a dummy probe was placed inside the cannula until the test day. A 3-mm-long active dialysis probe was perfused with Ringer's solution [147.2 mM NaCl, 4.0 mM KCl, and 2.2 mM $CaCl_2$ (pH 6.0); Fuso Pharmaceutical Industries, Osaka, Japan] at a constant flow rate of 1 μl/min. Microdialysates (20 μl) were collected every 20 min and injected immediately onto a high-performance liquid chromatograph equipped with an electrochemical detector (HTEC-500; Eicom) to assay the catecholamine levels. Three samples were collected to determine average basal catecholamine levels before injecting mice with CNO (1 mg/kg). After the experiments, Evans blue dye (FUJIFILM Wako Pure Chemical) was microinjected through the cannula to histologically verify the position of the probe. For simultaneous assaying of catecholamines, an Eicompak CAX column (2.0 mm inner diameter by 200 mm length; Eicom) was used, and the potential of the graphite electrode (Eicom) was set to +450 mV against that of an Ag/AgCl reference electrode. The mobile phase consisted of 100 mM ammonium acetate buffer (pH 6.0; 100 mM ammonium acetate and 100 mM acetic acid, FUJIFILM Wako Pure Chemical), 45 mM sodium sulfate (Nacalai Tesque), 134 μM ethylenediaminetetraacetic acid (DOJINDO, Kumamoto, Japan), and 24 v/v% methanol (Nacalai Tesque).

Pharmacological treatments

Mice received an intraperitoneal injection of the D1 dopamine receptor antagonist SCH39166 (0.02 mg/kg; Tocris Bioscience, Bristol, UK), the D2 dopamine receptor antagonist raclopride (0.1 mg/kg; Tocris Bioscience), the α1-adrenergic receptor antagonist prazosin (1 mg/kg; Sigma-Aldrich), or the β-adrenergic receptor antagonist propranolol (10 mg/kg; Sigma-Aldrich) 30 min before the behavioral tests. SCH39166, raclopride, and prazosin were dissolved in saline containing 1% DMSO. Propranolol was dissolved in saline.

Neuronal tracing combined with activity-dependent genetic labeling

Activity-dependent genetic labeling was performed as described previously (*69*) with minor modifications. TRAP2 mice were unilaterally injected with 50 nl of a mixture of AAVrg-hSyn-DIO-EGFP ($\geq 7 \times 10^{12}$ particles/ml; a gift from B. Roth; Addgene viral prep no. 50457-AAVrg; http://n2t.net/addgene:50457; RRID: Addgene_50457) and AAVrg-hSyn-mCherry ($\geq 4 \times 10^{12}$ particles/ml) into the CLA for retrograde somatic labeling. One week later, mice received an intraperitoneal injection of 2 mg of TAM (Cayman Chemical) dissolved in a 1:9 (v/v) mixture of ethanol (FUJIFILM Wako Pure Chemical) and corn oil (Sigma-Aldrich) at 20 mg/ml. Six hours after TAM injection, the mice were exposed to a single session of DS and then kept in their home cages in a quiet place for 48 hours after TAM injection.

Wireless optogenetics stimulation

After injection with the AAVdj-CaMKIIα-DIO-Chronos-EGFP or AAVdj-CaMKIIα-DIO-EGFP into the BLA (stereotaxic coordinates: −1.4 mm anterior, ±3.3 mm lateral, and −4.5 mm ventral to the bregma), a bilateral light-emitting diode cannula (TeleLCD-B-3.1-250-4.6, Bio Research Center, Nagoya, Japan) was implanted into the CLA and attached to the skull with dental cement. Mice were habituated with dummy Teleopt receivers (2 g, TeleDummy, Bio Research Center) in their home cages at least for 3 days before behavioral tests, real-time place preference test, and 9-min session open-field test. Thirty minutes before each behavioral test, mice were anesthetized using 2.5 to 3.5% isoflurane to replace the dummy Teleopt receivers with the TeleR-2-P optical receivers (Bio Research Center) and allowed recovery in their home cages. Light output was manipulated with Teleopto remote controller (Bio Research Center). During the light-on epochs, 3 to 6 mW of light trains at 20 Hz, 5-ms pulses of blue light (470 nm) were delivered via the optical fiber.

Real-time place preference test

The real-time place preference test was performed as described previously (*70*) with minor modifications. A separate behavioral chamber (40 cm by 20 cm by 30 cm) was used for the place preference task, which contained two compartments (20 cm by 20 cm), one of which had opaque white walls and the other had opaque black walls. The compartment of black wall was paired with blue light stimulation when animals entered the compartment. The activity of the mouse was recorded using a video camera, and the total distance traveled and time spent in each compartment were analyzed using ANY-maze video-tracking software.

Open-field test with 3-min OFF-ON-OFF epochs

Twenty-four hours after the real-time place preference test, the mice were subjected to open-field test consisting of three 3-min epochs: light stimulation off, on, and off (OFF-ON-OFF epochs, 9 min total) as described previously (*7*). The activity of each mouse was recorded and analyzed as above.

Schematic anatomical structure

The schematic anatomical structure of the brain was redrawn according to the Franklin and Paxinos mouse brain atlas (*71*).

Statistical analysis

For comparisons among three or more groups, two-way analysis of variance (ANOVA) or two-way repeated-measures ANOVA was used where applicable. As a post hoc analysis, the Bonferroni multiple comparisons test or Dunnett multiple comparisons test was used. For comparisons between two groups, parametric unpaired *t* test or nonparametric Welch's *t* test was used where applicable. To measure correlations, Pearson's *r* (Pearson's correlation coefficient) was used. Detailed statistical analysis including sample size is indicated in the figure legends. The statistical significance level was set at $P < 0.05$. Statistical analyses were conducted using GraphPad Prism 7.04 (GraphPad Software, San Diego, CA).

Abbreviations for brain areas

Abbreviations used for brain areas are according to the Allen Brain Reference Atlas (http://atlas.brain-map.org/): See table S1.

SUPPLEMENTARY MATERIALS

Supplementary material for this article is available at https://science.org/doi/10.1126/sciadv.abi6375

View/request a protocol for this paper from *Bio-protocol*.

REFERENCES AND NOTES

1. E. J. Hermans, M. J. A. Henckens, M. Joëls, G. Fernández, Dynamic adaptation of large-scale brain networks in response to acute stressors. *Trends Neurosci.* **37**, 304–314 (2014).
2. S. J. Lupien, B. S. McEwen, M. R. Gunnar, C. Heim, Effects of stress throughout the lifespan on the brain, behaviour and cognition. *Nat. Rev. Neurosci.* **10**, 434–445 (2009).
3. C. Gross, R. Hen, The developmental origins of anxiety. *Nat. Rev. Neurosci.* **5**, 545–552 (2004).
4. J. G. McCall, R. Al-Hasani, E. R. Siuda, D. Y. Hong, A. J. Norris, C. P. Ford, M. R. Bruchas, CRH engagement of the locus coeruleus noradrenergic system mediates stress-induced anxiety. *Neuron* **87**, 605–620 (2015).
5. B. S. McEwen, C. Nasca, J. D. Gray, Stress effects on neuronal structure: Hippocampus, amygdala, and prefrontal cortex. *Neuropsychopharmacology* **41**, 3–23 (2016).
6. K. M. Tye, R. Prakash, S. Y. Kim, L. E. Fenno, L. Grosenick, H. Zarabi, K. R. Thompson, V. Gradinaru, C. Ramakrishnan, K. Deisseroth, Amygdala circuitry mediating reversible and bidirectional control of anxiety. *Nature* **471**, 358–362 (2011).
7. A. C. Felix-Ortiz, A. Beyeler, C. Seo, C. A. Leppla, C. P. Wildes, K. M. Tye, BLA to vHPC inputs modulate anxiety-related behaviors. *Neuron* **79**, 658–664 (2013).
8. P. Tovote, J. P. Fadok, A. Luthi, Neuronal circuits for fear and anxiety. *Nat. Rev. Neurosci.* **16**, 317–331 (2015).
9. J. Gründemann, Y. Bitterman, T. Lu, S. Krabbe, B. F. Grewe, M. J. Schnitzer, A. Lüthi, Amygdala ensembles encode behavioral states. *Science* **364**, eaav8736 (2019).
10. G. G. Calhoon, K. M. Tye, Resolving the neural circuits of anxiety. *Nat. Neurosci.* **18**, 1394–1404 (2015).
11. M. E. Joffe, C. I. Santiago, K. H. Oliver, J. Maksymetz, N. A. Harris, J. L. Engers, C. W. Lindsley, D. G. Winder, P. J. Conn, $mGlu_2$ and $mGlu_3$ negative allosteric modulators divergently enhance thalamocortical transmission and exert rapid antidepressant-like effects. *Neuron* **105**, 46–59.e3 (2020).
12. K. Seiriki, A. Kasai, T. Hashimoto, W. Schulze, M. Niu, S. Yamaguchi, T. Nakazawa, K. I. Inoue, S. Uezono, M. Takada, Y. Naka, H. Igarashi, M. Tanuma, J. A. Waschek, Y. Ago, K. F. Tanaka, A. Hayata-Takano, K. Nagayasu, N. Shintani, R. Hashimoto, Y. Kunii, M. Hino, J. Matsumoto, H. Yabe, T. Nagai, K. Fujita, T. Matsuda, K. Takuma, A. Baba, H. Hashimoto, High-speed and scalable whole-brain imaging in rodents and primates. *Neuron* **94**, 1085–1100.e6 (2017).
13. K. Seiriki, A. Kasai, T. Nakazawa, M. Niu, Y. Naka, M. Tanuma, H. Igarashi, K. Yamaura, A. Hayata-Takano, Y. Ago, H. Hashimoto, Whole-brain block-face serial microscopy tomography at subcellular resolution using FAST. *Nat. Protoc.* **14**, 1509–1529 (2019).
14. K. Matsumura, K. Seiriki, S. Okada, M. Nagase, S. Ayabe, I. Yamada, T. Furuse, H. Shibuya, Y. Yasuda, H. Yamamori, M. Fujimoto, K. Nagayasu, K. Yamamoto, K. Kitagawa, H. Miura, N. Gotoda-Nishimura, H. Igarashi, M. Hayashida, M. Baba, M. Kondo, S. Hasebe, K. Ueshima, A. Kasai, Y. Ago, A. Hayata-Takano, N. Shintani, T. Iguchi, M. Sato, S. Yamaguchi, M. Tamura, S. Wakana, A. Yoshiki, A. M. Watabe, H. Okano, K. Takuma, R. Hashimoto, H. Hashimoto, T. Nakazawa, Pathogenic POGZ mutation causes impaired cortical development and reversible autism-like phenotypes. *Nat. Commun.* **11**, 859 (2020).
15. M. Eguchi, S. Yamaguchi, In vivo and in vitro visualization of gene expression dynamics over extensive areas of the brain. *Neuroimage* **44**, 1274–1283 (2009).
16. B. S. McEwen, N. P. Bowles, J. D. Gray, M. N. Hill, R. G. Hunter, I. N. Karatsoreos, C. Nasca, Mechanisms of stress in the brain. *Nat. Neurosci.* **18**, 1353–1363 (2015).
17. L. Liu, X. Zhou, Y. Zhang, J. Pu, L. Yang, S. Yuan, L. Zhao, C. Zhou, H. Zhang, P. Xie, Hippocampal metabolic differences implicate distinctions between physical and psychological stress in four rat models of depression. *Transl. Psychiatry* **8**, 4 (2018).
18. Y. Goll, G. Atlan, A. Citri, Attention: The claustrum. *Trends Neurosci.* **38**, 486–495 (2015).
19. Q. Wang, L. Ng, J. A. Harris, D. Feng, Y. Li, J. J. Royall, S. W. Oh, A. Bernard, S. M. Sunkin, C. Koch, H. Zeng, Organization of the connections between claustrum and cortex in the mouse. *J. Comp. Neurol.* **525**, 1317–1346 (2017).
20. B. N. Mathur, R. M. Caprioli, A. Y. Deutch, Proteomic analysis illuminates a novel structural definition of the claustrum and insula. *Cereb. Cortex* **19**, 2372–2379 (2009).
21. J. B. Smith, K. D. Alloway, P. R. Hof, R. Orman, D. H. Reser, A. Watakabe, G. D. R. Watson, The relationship between the claustrum and endopiriform nucleus: A perspective towards consensus on cross-species homology. *J. Comp. Neurol.* **527**, 476–499 (2019).
22. L. A. DeNardo, C. D. Liu, W. E. Allen, E. L. Adams, D. Friedmann, L. Fu, C. J. Guenthner, M. Tessier-Lavigne, L. Luo, Temporal evolution of cortical ensembles promoting remote memory retrieval. *Nat. Neurosci.* **22**, 460–469 (2019).
23. M. M. Brzozka, T. Unterbarnscheidt, M. H. Schwab, M. J. Rossner, OSO paradigm—A rapid behavioral screening method for acute psychosocial stress reactivity in mice. *Neuroscience* **314**, 1–11 (2016).
24. J. L. Gomez, J. Bonaventura, W. Lesniak, W. B. Mathews, P. Sysa-Shah, L. A. Rodriguesz, R. J. Ellis, C. T. Rischie, B. K. Harvey, R. F. Dannals, M. G. Pomper, A. Bonci, M. Michaelides, Chemogenetics revealed DREADD occupancy and activation via converted clozapine. *Science* **357**, 503–507 (2017).
25. B. Zingg, H. W. Dong, H. W. Tao, L. I. Zhang, Input-output organization of the mouse claustrum. *J. Comp. Neurol.* **526**, 2428–2443 (2018).
26. K. Narikiyo, R. Mizuguchi, A. Ajima, M. Shiozaki, H. Hamanaka, J. P. Johansen, K. Mori, Y. Yoshihara, The claustrum coordinates cortical slow-wave activity. *Nat. Neurosci.* **23**, 741–753 (2020).
27. A. F. T. Arnsten, Stress signalling pathways that impair prefrontal cortex structure and function. *Nat. Rev. Neurosci.* **10**, 410–422 (2009).
28. R. H. Roth, S. Y. Tam, Y. Ida, J. X. Yang, A. Y. Deutch, Stress and the mesocorticolimbic dopamine systems. *Ann. N. Y. Acad. Sci.* **537**, 138–147 (1988).
29. J. M. Finlay, M. J. Zigmond, E. D. Abercrombie, Increased dopamine and norepinephrine release in medial prefrontal cortex induced by acute and chronic stress: Effects of diazepam. *Neuroscience* **64**, 619–628 (1995).
30. J. Kim, M. Pignatelli, S. Xu, S. Itohara, S. Tonegawa, Antagonistic negative and positive neurons of the basolateral amygdala. *Nat. Neurosci.* **19**, 1636–1646 (2016).
31. U. S. Donges, H. Kugel, A. Stuhrmann, D. Grotegerd, R. Redlich, V. Lichev, N. Rosenberg, K. Ihme, T. Suslow, U. Dannlowski, Adult attachment anxiety is associated with enhanced automatic neural response to positive facial expression. *Neuroscience* **220**, 149–157 (2012).
32. O. Zinchenko, Brain responses to social punishment: A meta-analysis. *Sci. Rep.* **9**, 12800 (2019).
33. S. Ons, O. Marti, A. Armario, Stress-induced activation of the immediate early gene Arc (activity-regulated cytoskeleton-associated protein) is restricted to telencephalic areas in the rat brain: Relationship to c-fos mRNA. *J. Neurochem.* **89**, 1111–1118 (2004).
34. F. C. Crick, C. Koch, What is the function of the claustrum? *Philos. Trans. R. Soc. B Biol. Sci.* **360**, 1271–1279 (2005).
35. D. H. Zald, J. V. Pardo, The neural correlates of aversive auditory stimulation. *Neuroimage* **16**, 746–753 (2002).
36. T. Agren, J. Engman, A. Frick, J. Björkstrand, E. Larsson, T. Furmark, M. Fredrikson, Disruption of reconsolidation erases a fear memory trace in the human amygdala. *Science* **337**, 1550–1552 (2012).
37. J. Jackson, M. M. Karnani, B. V. Zemelman, D. Burdakov, A. K. Lee, Inhibitory control of prefrontal cortex by the claustrum. *Neuron* **99**, 1029–1039.e4 (2018).
38. E. Likhtik, J. M. Stujenske, M. A. Topiwala, A. Z. Harris, J. A. Gordon, Prefrontal entrainment of amygdala activity signals safety in learned fear and innate anxiety. *Nat. Neurosci.* **17**, 106–113 (2014).
39. S. Kumar, R. Hultman, D. Hughes, N. Michel, B. M. Katz, K. Dzirasa, Prefrontal cortex reactivity underlies trait vulnerability to chronic social defeat stress. *Nat. Commun.* **5**, 4537 (2014).
40. O. Bukalo, C. Pinard, S. Silverstein, C. Brehm, N. D. Hartley, N. Whittle, G. Caolacicco, E. Busch, S. Patel, N. Singewald, A. Holmes, Prefrontal inputs to the amygdala instruct fear extinction memory formation. *Sci. Adv.* **1**, e1500251 (2015).
41. J. Jackson, J. B. Smith, A. K. Lee, The anatomy and physiology of claustrum-cortex interactions. *Annu. Rev. Neurosci.* **43**, 231–247 (2020).
42. Z. Chia, G. J. Augustine, G. Silberberg, Synaptic connectivity between the cortex and claustrum is organized into functional modules. *Curr. Biol.* **30**, 2777–2790.e4 (2020).
43. A. Terem, B. J. Gonzales, N. Peretz-Rivlin, R. Ashwal-Fluss, N. Bleistein, M. Del Mar Reus-Garcia, D. Mukherjee, M. Groysman, A. Citri, Claustral neurons projecting to frontal cortex mediate contextual association of reward. *Curr. Biol.* **30**, 3522–3532.e6 (2020).
44. S. R. Krimmel, M. G. White, M. H. Panicker, F. S. Barrett, B. N. Mathur, D. A. Seminowicz, Resting state functional connectivity and cognitive task-related activation of the human claustrum. *Neuroimage* **196**, 59–67 (2019).
45. M. A. Ungless, Dopamine: The salient issue. *Trends Neurosci.* **27**, 702–706 (2004).
46. S. Puglisi-Allegra, R. Ventura, Prefrontal/accumbal catecholamine system processes high motivational salience. *Front. Behav. Neurosci.* **6**, 31 (2012).
47. K. Tanaka, T. Furuyashiki, S. Kitaoka, Y. Senzai, Y. Imoto, E. Segi-Nishida, Y. Deguchi, R. M. Breyer, M. D. Breyer, S. Narumiya, Prostaglandin E2-mediated attenuation of mesocortical dopaminergic pathway is critical for susceptibility to repeated social defeat stress in mice. *J. Neurosci.* **32**, 4319–4329 (2012).
48. M. Pignatelli, A. Bonci, Role of dopamine neurons in reward and aversion: A synaptic plasticity perspective. *Neuron* **86**, 1145–1157 (2015).
49. V. Krishnan, M. H. Han, D. L. Graham, O. Berton, W. Renthal, S. J. Russo, Q. Laplant, A. Graham, M. Lutter, D. C. Lagace, S. Ghose, R. Reister, P. Tannous, T. A. Green, R. L. Neve, S. Chakravarty, A. Kumar, A. J. Eisch, D. W. Self, F. S. Lee, C. A. Tamminga, D. C. Cooper, H. K. Gershenfeld, E. J. Nestler, Molecular adaptations underlying susceptibility and resistance to social defeat in brain reward regions. *Cell* **131**, 391–404 (2007).
50. M. G. White, C. Mu, H. Qadir, M. B. Madden, H. Zeng, B. N. Mathur, The mouse claustrum is required for optimal behavioral performance under high cognitive demand. *Biol. Psychiatry* **88**, 719–726 (2020).

51. T. Kitanishi, N. Matsuo, Organization of the claustrum-to-entorhinal cortical connection in mice. *J. Neurosci.* **37**, 269–280 (2017).
52. O. Berton, C. A. McClung, R. J. Dileone, V. Krishnan, W. Renthal, S. J. Russo, D. Graham, N. M. Tsankova, C. A. Bolanos, M. Rios, L. M. Monteggia, D. W. Self, E. J. Nestler, Essential role of BDNF in the mesolimbic dopamine pathway in social defeat stress. *Science* **311**, 864–868 (2006).
53. M. Niu, A. Kasai, K. Seiriki, M. Hayashida, M. Tanuma, R. Yokoyama, Y. Hirato, H. Hashimoto, Altered functional connectivity of the orbital cortex and striatum associated with catalepsy induced by Dopamine D1 and D2 antagonists. *Biol. Pharm. Bull.* **44**, 442–447 (2021).
54. A. Abraham, F. Pedregosa, M. Eickenberg, P. Gervais, A. Mueller, J. Kossaifi, A. Gramfort, B. Thirion, G. Varoquaux, Machine learning for neuroimaging with scikit-learn. *Front. Neuroinform.* **8**, 14 (2014).
55. R. Tibshirani, Regression shrinkage and selection via the lasso. *J. R. Stat. Soc. Ser. B* **58**, 267–288 (1996).
56. H. A. Sturges, The choice of a class interval. *J. Am. Stat. Assoc.* **21**, 65–66 (1926).
57. K. Hazama, A. Hayata-Takano, K. Uetsuki, A. Kasai, N. Encho, N. Shintani, K. Nagayasu, R. Hashimoto, D. Reglodi, T. Miyakawa, T. Nakazawa, A. Baba, H. Hashimoto, Increased behavioral and neuronal responses to a hallucinogenic drug in PACAP heterozygous mutant mice. *PLOS ONE* **9**, e89153 (2014).
58. A. Inutsuka, A. Inui, S. Tabuchi, T. Tsunematsu, M. Lazarus, A. Yamanaka, Concurrent and robust regulation of feeding behaviors and metabolism by orexin neurons. *Neuropharmacology* **85**, 451–460 (2014).
59. L. Reijmers, B. Perkins, N. Matsuo, M. Mayford, Localization of a stable neural correlate of associative memory. *Science* **317**, 1230–1233 (2007).
60. T. Matsuda, C. Cepko, Controlled expression of transgenes introduced by in vivo electroporation. *Proc. Natl. Acad. Sci. U.S.A.* **104**, 1027–1032 (2007).
61. N. Asaoka, N. Nishitani, H. Kinoshita, Y. Nagai, H. Hatakama, K. Nagayasu, H. Shirakawa, T. Nakagawa, S. Kaneko, An adenosine A_{2A} receptor antagonist improves multiple symptoms of repeated quinpirole-induced psychosis. *eNeuro* **6**, ENEURO.e0366-18.2019 (2019).
62. D. G. Tervo, B. Y. Hwang, S. Viswanathan, T. Gaj, M. Lavzin, K. D. Ritola, S. Lindo, S. Michael, E. Kuleshova, D. Ojala, C. C. Huang, C. R. Gerfen, J. Schiller, J. T. Dudman, A. W. Hantman, L. L. Looger, D. V. Schaffer, A. Y. Karpova, A designer AAV variant permits efficient retrograde access to projection neurons. *Neuron* **92**, 372–382 (2016).
63. B. Armbruster, X. Li, M. Pausch, S. Herlitze, B. Roth, Evolving the lock to fit the key to create a family of G protein-coupled receptors potently activated by an inert ligand. *Proc. Natl. Acad. Sci. U.S.A.* **104**, 5163–5168 (2007).
64. H. Hashimoto, N. Shintani, K. Tanaka, W. Mori, M. Hirose, T. Matsuda, M. Sakaue, J. Miyazaki, H. Niwa, F. Tashiro, K. Yamamoto, K. Koga, S. Tomimoto, A. Kunugi, S. Suetake, A. Baba, Altered psychomotor behaviors in mice lacking pituitary adenylate cyclase-activating polypeptide (PACAP). *Proc. Natl. Acad. Sci. U.S.A.* **98**, 13355–13360 (2001).
65. S. A. Golden, H. E. Covington III, O. Berton, S. J. Russo, A standardized protocol for repeated social defeat stress in mice. *Nat. Protoc.* **6**, 1183–1191 (2011).
66. Y. Ago, W. Tanabe, M. Higuchi, S. Tsukada, T. Tanaka, T. Yamaguchi, H. Igarashi, R. Yokoyama, K. Seiriki, A. Kasai, T. Nakazawa, S. Nakagawa, K. Hashimoto, H. Hashimoto, (R)-ketamine induces a greater increase in prefrontal 5-HT release than (S)-ketamine and ketamine metabolites via an AMPA receptor-independent mechanism. *Int. J. Neuropsychopharmacol.* **22**, 665–674 (2019).
67. C. Menard, M. L. Pfau, G. E. Hodes, V. Kana, V. X. Wang, S. Bouchard, A. Takahashi, M. E. Flanigan, H. Aleyasin, K. B. LeClair, W. G. Janssen, B. Labonte, E. M. Parise, Z. S. Lorsch, S. A. Golden, M. Heshmati, C. Tamminga, G. Turecki, M. Campbell, Z. A. Fayad, C. Y. Tang, M. Merad, S. J. Russo, Social stress induces neurovascular pathology promoting depression. *Nat. Neurosci.* **20**, 1752–1760 (2017).
68. Y. Ago, R. Araki, T. Tanaka, A. Sasaga, S. Nishiyama, K. Takuma, T. Matsuda, Role of social encounter-induced activation of prefrontal serotonergic systems in the abnormal behaviors of isolation-reared mice. *Neuropsychopharmacology* **38**, 1535–1547 (2013).
69. C. M. Root, C. A. Denny, R. Hen, R. Axel, The participation of cortical amygdala in innate, odour-driven behaviour. *Nature* **515**, 269–273 (2014).
70. R. Chen, F. Gore, Q. A. Nguyen, C. Ramakrishnan, S. Patel, S. H. Kim, M. Raffiee, Y. S. Kim, B. Hsueh, E. Krook-Magnusson, I. Soltesz, K. Deisseroth, Deep brain optogenetics without intracranial surgery. *Nat. Biotechnol.* **39**, 161–164 (2021).
71. K. B. J. Franklin, G. Paxinos, *The Mouse Brain: In Stereotaxic Coordinates. Compact third edition* (Academic Press, 2008).
72. J. B. Smith, G. D. R. Watson, Z. Liang, Y. Liu, N. Zhang, K. D. Alloway, A role for the claustrum in salience processing? *Front. Neuroanat.* **13**, 64 (2019).
73. K. Y. Chan, M. J. Jang, B. B. Yoo, A. Greenbaum, N. Ravi, W. L. Wu, L. Sanchez-Guardado, C. Lois, S. K. Mazmanian, B. E. Deverman, V. Gradinaru, Engineered AAVs for efficient noninvasive gene delivery to the central and peripheral nervous systems. *Nat. Neurosci.* **20**, 1172–1179 (2017).
74. S. Picelli, O. R. Faridani, A. K. Bjorklund, G. Winberg, S. Sagasser, R. Sandberg, Full-length RNA-seq from single cells using Smart-seq2. *Nat. Protoc.* **9**, 171–181 (2014).
75. M. Martin, Cutadapt removes adapter sequences from high-throughput sequencing reads. *EMBnet J.* **17**, 10–12 (2011).
76. B. Langmead, S. L. Salzberg, Fast gapped-read alignment with Bowtie 2. *Nat. Methods* **9**, 357–359 (2012).
77. D. Kim, B. Langmead, S. L. Salzberg, HISAT: A fast spliced aligner with low memory requirements. *Nat. Methods* **12**, 357–360 (2015).
78. Y. Liao, G. K. Smyth, W. Shi, featureCounts: An efficient general purpose program for assigning sequence reads to genomic features. *Bioinformatics* **30**, 923–930 (2014).
79. K. Van den Berge, F. Perraudeau, C. Soneson, M. I. Love, D. Risso, J. P. Vert, M. D. Robinson, S. Dudoit, L. Clement, Observation weights unlock bulk RNA-seq tools for zero inflation and single-cell applications. *Genome Biol.* **19**, 24 (2018).
80. M. I. Love, W. Huber, S. Anders, Moderated estimation of fold change and dispersion for RNA-seq data with DESeq2. *Genome Biol.* **15**, 550 (2014).
81. J. Alquicira-Hernandez, A. Sathe, H. P. Ji, Q. Nguyen, J. E. Powell, *scPred*: Accurate supervised method for cell-type classification from single-cell RNA-seq data. *Genome Biol.* **20**, 264 (2019).

Acknowledgments: We dedicate this paper to R. S. Duman (Yale University School of Medicine, New Haven, CT), who provided us with invaluable suggestions and motivated us. We wish to thank J. P. Johansen (RIKEN Center for Brain Science, Saitama, Japan) for critical comments on the manuscript. We are grateful to M. Eguchi (Gifu University Department of Medicine, Gifu, Japan) for support on the Arc-dVenus reporter mice. Computations were partially performed on the NIG supercomputer at ROIS National Institute of Genetics. **Funding:** This work was supported in part by JSPS KAKENHI grant numbers JP19K07121 (H.H.), JP20H00492 (H.H.), JP20H03429 (H.H.), JP20K07736 (H.H.), JP21K19335 (H.H.), JP17H05054 (A.K.), JP18H05132 (A.K.), JP18K19399 (A.K.), JP19H05217 (A.K.), JP20H03391 (A.K.), JP20H05065 (A.K.), JP19H05218 (T.N.), JP19H04910 (K. Sei.), JP19H05020 (K. Sei.), JP20H03556 (K. Sei.), JP20H04774 (K.N.), JP20K07064 (K.N.), JP18H04616 (S.K.), JP20H00491 (S.K.), JP18J10350 (M.N.), and JP20J20247 (M. Tan.); MEXT KAKENHI grant number JP18H05416 (H.H.); AMED grant numbers JP20dm0107122 (H.H.), JP20dm0207061 (H.H.), JP21am0101084 (H.H.), JP21dm0207117 (H.H.), JP18jm0610007 (A.K.), JP21wm0425017 (A.K.), JP20ak0101088 (S.K.), JP20dm0207003 (M. Tak.), and JP20dm0307021 (K.I.); JST grant number JPMJFR2061 (A.K.); and grants from the Takeda Science Foundation, Japan (A.K., T.N., and H.H.), the Mochida Memorial Foundation for Medical and Pharmaceutical Research, Japan (A.K.), and the Hoansha Foundation, Japan (A.K.). **Author contributions:** A.K. and H.H. conceived and designed the study; M.N., M. Tan., K. Sei., H.I., T.K., K.M., H.U., W.T., K. Seo, R.Y., and J.O. performed the experiments with help from S.K., Y.A., T.N., and H.O.; M.N., A.K., M. Tan., K. Sei., H.I., and H.H. performed the image analyses; K. Sei., H.I., K.N., M.H., and S.K. performed the computational analyses; K.I., M. Tak., S.Y., and A.Y. provided the methodology and tools; T.N. provided advice on experimental designs and interpretation of the data; and M.N., A.K., and H.H. wrote the manuscript with input from all coauthors. **Competing interests:** The authors declare that they have no competing interests. **Data and materials availability:** All data needed to evaluate the conclusions in the paper are present in the paper and/or the Supplementary Materials. The raw data of single-cell RNA sequence and AAV transgenes can be provided by A.K. pending scientific review and a completed material transfer agreement. Requests for these materials should be submitted to kasai@phs.osaka-u.ac.jp.

Submitted 22 March 2021
Accepted 26 January 2022
Published 18 March 2022
10.1126/sciadv.abi6375